Chemical Engineering Science 65 (2010) 527–537

Contents lists available at ScienceDirect

Chemical Engineering Science

journal homepage: www.elsevier.com/locate/ces

Volume-of-fluid (VOF) simulations of rise of single/multiple bubbles in sheared liquids

Swapna S. Rabha, Vivek V. Buwa*

Department of Chemical Engineering, Indian Institute of Technology-Delhi, New Delhi 110 016, India

ARTICLE INFO

Article history:
Received 7 July 2008
Received in revised form 14 June 2009
Accepted 20 June 2009
Available online 26 June 2009

Keywords:
Bubble
Lift force
Simulation
Volume-of-fluid method
Homogeneous bubbly flow
Heterogeneous bubbly flow

ABSTRACT

The understanding of the lift force, which governs the lateral migration of bubbles, is important to improve closures for continuum flow models that are used to simulate large-scale dispersed gas–liquid flows. In the present work, the effect of bubble size/shape and more importantly the effect of neighboring bubbles on the magnitude and direction of the lift force were investigated. The rise behavior of single/multiple bubbles in liquids of different properties imposed with linear shear was simulated by using the VOF method. The predicted lift coefficients (C_L) for single bubbles rising in sheared viscous liquid (corresponding to the ellipsoidal regime, $2.35 \leq Eo \leq 11.68$, $\log Mo = -5.3$) were compared with the measurement of Tomiyama et al. [2002. Transverse migration of single bubbles in simple shear flows. Chemical Engineering Science 57, 1849–1858]. Further, the lift force acting on single bubbles rising in low viscosity liquid (corresponding to the wobbling regime, $1.1 \leq Eo \leq 8.72$, $-10.6 \leq \log Mo \leq -14.6$) was investigated. Unlike the steady lateral migration of single bubbles with a single characteristics value of C_L (+ve or −ve depending on d_B) for viscous systems, the bubbles were found oscillate around the center line and the instantaneous C_L was found to fluctuate in both +ve and −ve directions. The effect of neighboring bubbles on the lift force was investigated by simulating the rise of six homogeneous (mono-dispersed) and heterogeneous (poly-dispersed) bubbles in a viscous liquid. It was observed that individual bubble wakes led to increased bubble–bubble interaction and as a result fluctuations in C_L were increased. The time-averaged C_L of all the bubbles was found to be very small as compared to the characteristic C_L obtained for the single bubble rise. These observations confirm the hypothesis of Beyerlein et al. [1985. Prediction of bubble concentration profiles in vertical turbulent two-phase flow. International Journal of Multiphase Flow 11, 629–641] and Behzadi et al. [2004. Modelling of dispersed bubble and droplet flow at high phase fractions. Chemical Engineering Science 59, 759–770] that C_L approaches to a very small value with moderate increases in the volume fraction.

1. Introduction

Several engineering processes involve gas–liquid flows, for example, in chemical processing, oil and gas industries, biochemical operations, etc. Bubble columns and stirred vessels are a few of the most widely used gas–liquid contactors/reactors. Last decade witnessed the development of numerical methods based on the continuum (Euler/Euler) and the discrete particle (Euler/Lagrange) approaches to simulate unsteady, dispersed gas–liquid flows in above mentioned gas–liquid reactors. In both the approaches, the momentum exchange between the two phases is accounted by a source term $\vec{F}_{GL}$ in the momentum equation which is calculated as the summation of the various inter-phase forces, e.g. drag ($\vec{F}_D$), lift ($\vec{F}_L$) and virtual mass ($\vec{F}_{VM}$) forces.

Though the models based on the above-mentioned approaches can predict the time-averaged and dynamics characteristics of gas–liquid flows quantitatively well for simple systems with low gas hold-ups (homogeneous bubbly flow) (e.g. Buwa and Ranade, 2002; Rampure et al., 2003), the quantitative predictions of gas–liquid flows with higher gas hold-up (observed for superficial gas velocities $> 20\,\mathrm{cm\,s^{-1}}$) are still out of reach. This is primarily because of the lack of adequate closure models that can account for the effect of bubble shape/size on different forces acting on a bubble and more importantly the influence of neighboring bubbles (or gas hold-up) on the inter-phase forces. In literature, there exist several correlations to estimate drag force acting on single bubbles of varying size and, shape (Clift et al., 1978; Krishna et al., 1999). The effect of gas hold-up on the drag coefficient obtained for a single bubble (C_{D0}) is often accounted by applying empirical corrections (e.g. proposed by

* Corresponding author. Tel.: +91 11 2659 1027; fax: +91 11 2658 1120.
E-mail address: vvbuwa@chemical.iitd.ac.in (V.V. Buwa).

0009-2509/$ - see front matter © 2009 Elsevier Ltd. All rights reserved.
doi:10.1016/j.ces.2009.06.061

Ishii and Zuber, 1979 or more recently by Behzadi et al., 2004). While several research groups are investigating the effects of neighboring bubbles (or gas hold-up) on bubble rise velocities (Bunner and Tryggvason, 2002) and on drag coefficient (Sankaranarayanan et al., 2002; Behzadi et al., 2004), the understanding of the lift force acting on single bubbles of different size and shapes and particularly the influence of neighboring bubbles on the lift coefficient is lacking to a large extent. The present work is therefore focused on numerical investigations of lift force acting on single and multiple bubbles.

In most of the macroscopic two-fluid simulations, only the drag force was taken into account and it therefore received more attention than that of the lift force. But in systems where velocity gradients in the liquid phase exist, lift force plays a crucial role in determining the lateral migration of bubbles. The lift force exerted on a single bubble rising in a liquid is generated by three different mechanisms: Magnus lift due to bubble rotation (Magnus, 1853), Saffman lift due to shear in the liquid (Saffman, 1965) and wake induced lift (Kariyasaki, 1987) (for further detail see Rafique et al., 2003). The shear-induced lift force ($\vec{F}_L$) is defined as (Žun, 1980; Auton, 1987):

$$\vec{F}_L = -C_L \rho_L \frac{\pi d_B^2}{6}(\vec{V}_G - \vec{V}_L) \times (\nabla \times \vec{V}_L) \quad (1)$$

Several analytical, experimental and numerical studies were done to develop correlations for estimation of lift coefficient under different flow conditions characterized by dimensionless numbers: Eotvos (Eo), Reynolds (Re), Galileo (Ga) and Morton (Mo) numbers (reviewed by Rafique et al., 2003; Hibiki and Ishii, 2007). A brief review of the previous work on the lift coefficient of a single bubble rising in a sheared liquid is presented below.

Auton (1987) theoretically determined the value of C_L of 0.5 for a spherical bubble in an inviscid rotational flow. Kariyasaki (1987) performed experiments for viscous systems with linear shear flow and observed that deformed bubbles were found to migrate in the direction opposite to that of theoretical predictions for rigid spheres. Sridhar and Katz (1995) studied the lift force acting on bubbles entrained in vortices and found C_L to vary as the fourth root of the dimensionless vorticity. But the correlation proposed by Sridhar and Katz (1995) was valid for very small bubbles ($2.45 \times 10^{-3} < Eo < 8.7 \times 10^{-2}$, $\log Mo = -10.6$ and $Re = 20-80$) in rotational and invisid flows. Later, Tomiyama et al. (2002) performed experiments to estimate the lift force acting on single spherical/ellipsoidal air bubbles of different size ($2.8 \leq d_B \leq 5.68$ mm) rising in a simple shear flow ($0 \leq \omega \leq 6.2 s^{-1}$) of a viscous liquid ($\mu_L = 0.018 - 0.089\,\mathrm{kg\,m^{-1}\,s^{-1}}$). They showed that for smaller bubbles ($d_B < 4.4$ mm), the C_L was dependent on Re and for large bubbles ($d_B < 4.4$ mm), the C_L was independent on Re and Eo numbers. They proposed different correlations to calculate C_L for $Eo_H < 4$ and $4 \leq Eo_H \leq 10.7$, however, these correlations were valid only for viscous systems and their applicability for less viscous liquids (e.g. water) was not verified.

Legendre and Magnaudet (1998) performed DNS of a single spherical bubble rising in a viscous liquid imposed with linear shear flow for different $Re(0.1 < Re < 500)$ and ω (0.02 and $0.2\,s^{-1}$) and developed an empirical correlation for estimation of the lift coefficient. Later, Bothe et al. (2006) performed volume-of-fluid (VOF) simulations of bubbles ($2.8 \leq d_B \leq 10$ mm) rising in viscous liquid ($\mu_L = 0.018 - 0.1\,\mathrm{kg\,m^{-1}\,s^{-1}}$; $\sigma = 0.061 - 0.8\,\mathrm{N\,m^{-1}}$) imposed with linear shear corresponding to the experimental data reported by Tomiyama et al. (2002) and proposed a correlation for C_L as a linear function of the Eo_H. However, this correlation was valid for only high liquid viscosities ($4 \leq Eo_H \leq 8$, $-3.6 \leq \log Mo \leq -5.7$ and could not be used for less viscous liquids like water.

From the previous literature, it is clear that the bubble shape plays a very important role in determining the magnitude and direction of the lift force. It can also be noted that most of the above-mentioned correlations were developed for smaller bubbles ($1\,\mathrm{mm} < d_B < 6\,\mathrm{mm}$) and for viscous systems ($\mu_L > 0.019\,\mathrm{kg\,m^{-1}\,s^{-1}}$) that fall in spherical and ellipsoidal shape regime. However, the understanding of lift force acting on single bubbles of larger size ($d_B > 5$ mm) especially in low viscosity fluids (e.g. water) that fall in wobbling and spherical cap regime is lacking. While most of the experimental and numerical investigations were focused on the lift force acting on a single bubble, the rise behavior of a swarm of bubbles is different from that of a single bubble. The wake effects and bubble–bubble interactions greatly influence the bubble shapes and their rise velocities and consequently the inter-phase coupling forces. Beyerlein et al. (1985) investigated the lift force for an upward gas–liquid flow in a vertical pipe using the two-fluid model and corrected the lift coefficient empirically with the mean inlet phase fraction (α_d) as $C_L = 1.65 \times 10^{-3}\alpha_d^{-0.78}$ such that the predicted and measured radial gas volume fraction profiles were in a good agreement each other. It can be see from the correlation of Beyerlein et al. (1985) that the value of C_L approaches to zero even at the small volume fractions (~0.02).

Later, Behzadi et al. (2004) postulated that at higher volume fractions, bubbles would experience the vorticity generated by neighboring bubbles than directly experiencing the mean shear and modified the correlation proposed by Beyerlein et al. (1985). They further argued that the vorticity generated by the bubbles would weakly depend on the mean liquid velocity gradient, thereby diminishing the effect of the mean liquid velocity gradient on the lift force and emphasized the need for further investigations. Sankaranarayanan and Sundaresan (2002) developed a correlation for lift force acting on bubbles at different volume fractions in a periodic box using lattice-Boltzmann method and proposed the correction of $C_L = C_{L0}(1+8\alpha_d)$ for the lift force which was valid for $\alpha_d < 0.15$.

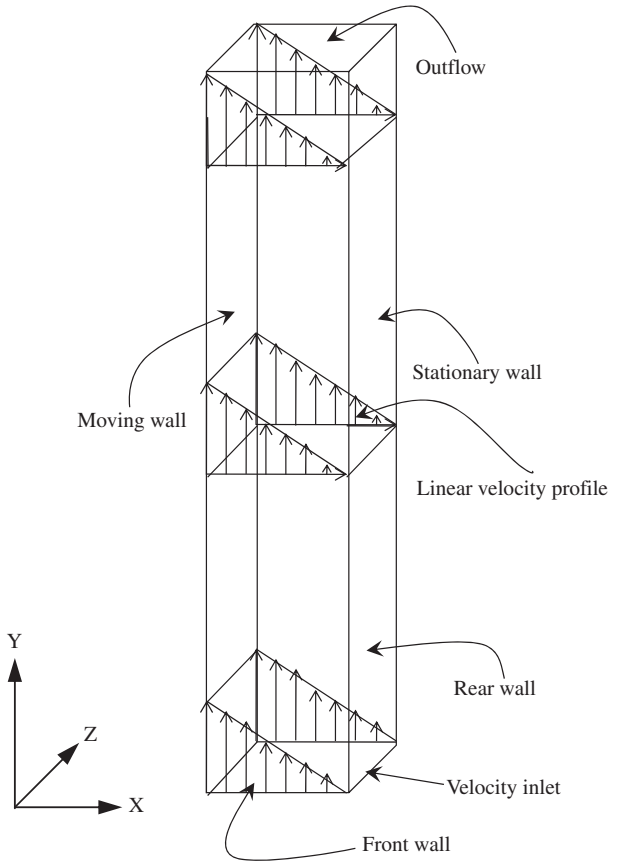

Fig. 1. Solution domain and boundary conditions.

Table 1
Range of parameter considered in the present work for single bubble rise.

Liquid	Water			Water–glycerol		
ρ_L(kg m^{-3})	1000			1154		
μ_L(kg m^{-1} s^{-1})	0.001			0.019		
σ(N m^{-1})	0.072			0.061		
log *Mo*	−10.6			−5.3		
w(s^{-1})	6.2			6.2		
d_B (mm)	2.85	5.54	8	3.52	5.54	8
Eo	1.1	4.17	8.72	2.35	5.68	11.68
Ga	2.27×10^2	1.668×10^3	5.022×10^3	1.587×10^3	6.157×10^3	1.852×10^4

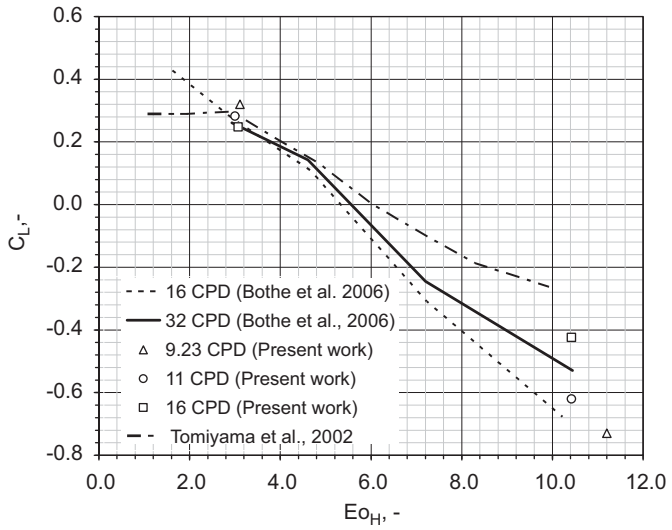

Fig. 2. Effect of grid resolution on the predicted C_L for a bubble with $d_B = 3.52$ mm ($Eo_H \sim 3$) and 5.54 mm ($Eo_H \sim 10.4$) rising in air–water+glycerol system ($\mu_L = 0.019$ kg m^{-1} s^{-1}). The predictions of Bothe et al. (2006) and measurements of Tomiyama et al. (2002) are also shown for comparison.

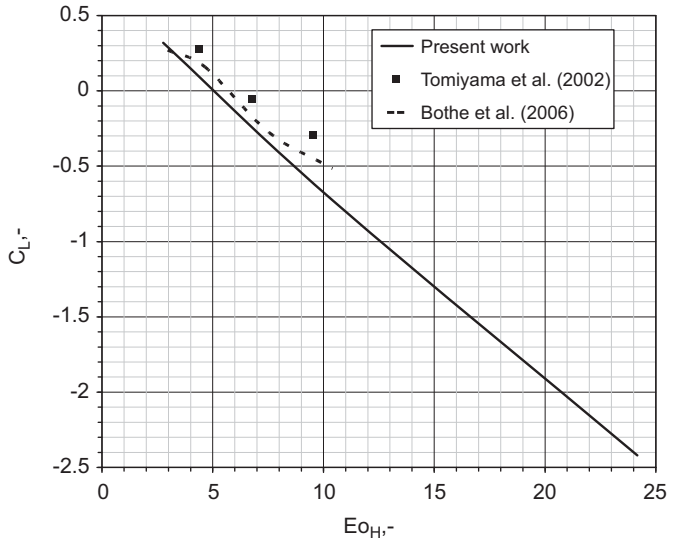

Fig. 3. Comparison of predicted C_L in the present work with the experiments of Tomiyama et al. (2002) and the predictions of Bothe et al. (2006) of an air bubble rising in a viscous liquid (Liquid: water+glycerol, $\omega = 6.2$ s^{-1})

It should be noted that the correction proposed by Sankaranarayanan and Sundaresan (2002) leads to increase in C_L with increase in α_d and that proposed by Beyerlein et al. (1985) (and latter the modified by Behzadi et al., 2004) leads to a sharp decrease in C_L with increase in α_d. Since in all of their simulations, Sankaranarayanan and Sundaresan (2002) considered a single bubble in a periodic box, their correlation for C_L is valid only for an ordered array of identical bubbles. However, bubbles undergo shape deformation leading to asymmetric vorticity distribution. In such cases, the effect of individual bubble wakes and the bubble–bubble interactions will be significant even for a mono-dispersed bubbly flow. To best of author's knowledge, the effect of bubble wakes and bubble interactions on the lift force experienced in a swarm of homogeneously and heterogeneously dispersed bubbles is not investigated before. The present work is aimed to provide this information.

In the present work, we report numerical investigations of lift force acting on both single and multiple bubbles in linear shear flow of liquids with different properties. For investigations on single bubbles, simulations were performed for ellipsoidal and wobbling bubbles of different sizes ($3\,\text{mm} \le d_B \le 8\,\text{mm}$) for both air–water+glycerol ($2.35 \le Eo \le 11.68$ and $\log Mo = -5.3$) and air–water ($2.35 \le Eo \le 11.68$ and $\log Mo = -10.6$). The predicted lift coefficients were compared with the experimental results of Tomiyama et al. (2002). The effect of neighboring bubbles on lift force was investigated by carrying out multiple bubbles simulations for both homogeneously and heterogeneously dispersed bubbles of to different diameters. A brief description of the volume-of-fluid (VOF) method, solution domain and boundary conditions used in the present work is provided in Section 2, the calculation of C_L from the simulated bubble trajectories is discussed in Section 3 and results are discussed in Section 4.

2. Computational model

In this study, the VOF method (Hirt and Nichols, 1981) was used to simulate the bubble rise behavior in sheared liquids. Gas and liquid phases were considered as incompressible fluids and the flow was assumed to be Newtonian and laminar.

2.1. The VOF method

In this method, a particular phase 'q' is identified by its volume fraction (α_q) in a computational cell. If $\alpha_q = 1$; the cell is full of the qth (secondary) phase; if $\alpha_q = 0$; the cell is full of the pth (primary) phase and if $0 < \alpha_q < 1$; the cell contains the interface between the pth and qth phases. A single set of Navier–Stokes equation for an incompressible Newtonian flow was solved:

$$\frac{\partial}{\partial t}(\rho\vec{v}) + \nabla.(\rho\vec{v}\vec{v}) = -\nabla p + \nabla[\mu(\nabla\vec{v} + (\nabla\vec{v})^T)] + \rho\vec{g} + \vec{F} \quad (2)$$

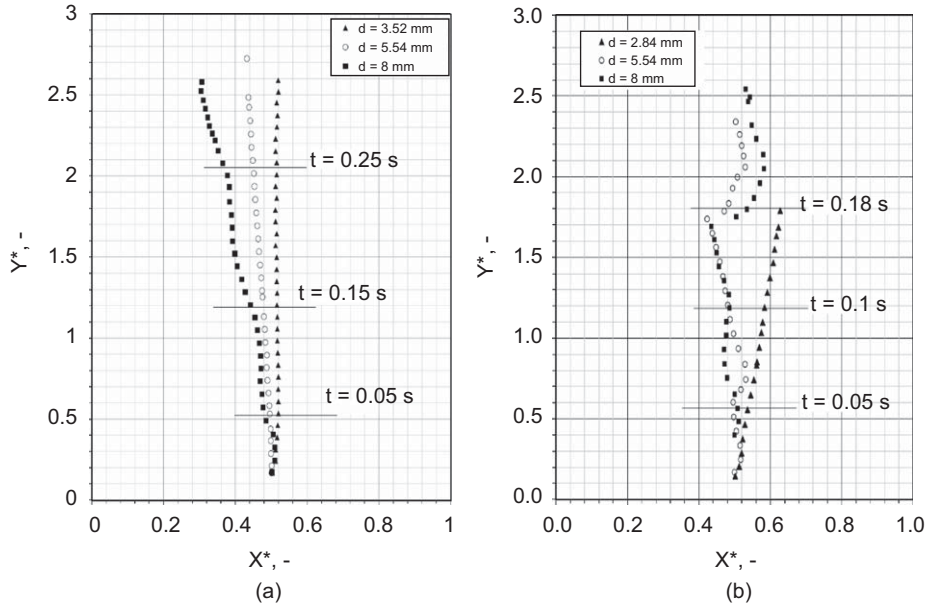

Fig. 4. Simulated bubble trajectories (a) air–water+glycerol ($\mu_L = 0.019\,\mathrm{kg\,m^{-1}\,s^{-1}}$) and (b) air–water ($\mu_L = 0.001\,\mathrm{kg\,m^{-1}\,s^{-1}}$).

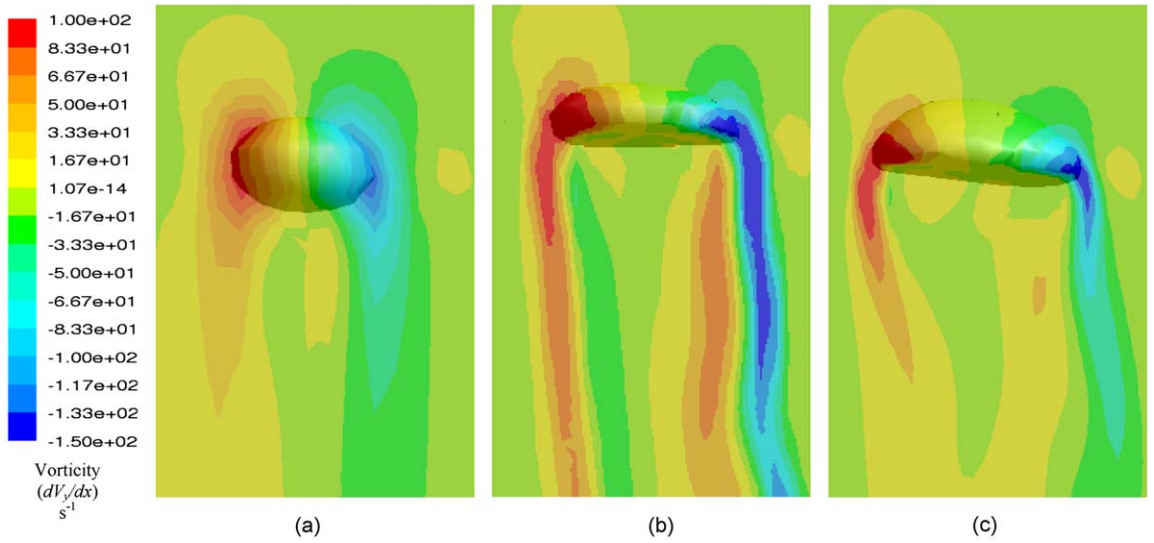

Fig. 5. Instantaneous bubble shapes and vorticity distributions for air bubbles rising in high viscosity liquid (water+glycerol, $\omega = 6.2\,\mathrm{s^{-1}}$) (a) $d_B = 3.52$ mm, (b) $d_B = 5.54$ mm and (c) $d_B = 8$ mm.

where $\vec{F}$ is the surface tension force per unit volume. When a computational cell is not entirely occupied by one phase, mixture properties (estimated by Eqs. (3) and (4)) were used to solve the Eq. (2):

$$\rho = \alpha_q \rho_q + (1 - \alpha_q)\rho_p \tag{3}$$

$$\mu = \alpha_q \mu_q + (1 - \alpha_q)\mu_p \tag{4}$$

The CSF model of Brackbill et al. (1992) was used to compute the surface tension force for the cells containing the gas–liquid interface:

$$\vec{F} = \sigma \frac{\rho \kappa n}{\frac{1}{2}(\rho_p + \rho_q)} \tag{5}$$

where σ is the coefficient of surface tension, $\hat{n}$ is the surface normal which is estimated from the gradient of volume fraction, κ is the local surface curvature calculated as follows (Brackbill et al., 1992).

$$\kappa = -(\nabla \hat{n}) = \frac{1}{|n|}\left[\frac{n}{|n|}\nabla|n| - (\nabla . n)\right] \tag{6}$$

The geometric reconstruction scheme based on the piecewise linear approach (Rider and Kothe, 1998) was used for the reconstruction of the interface. In the VOF approach, the reconstructed interface is advected by solving an advection equation for the volume fraction of the secondary phase. For the qth phase, advection equation is written as

$$\frac{\partial}{\partial t}(\alpha_q \rho_q) + \nabla.(\alpha_q \rho_q \vec{v}_q) = 0 \tag{7}$$

The primary phase volume fraction is computed from the relation: $\alpha_p + \alpha_q = 1$. Eqs (2) and (7) were solved using the commercial flow solver Fluent 6.2.

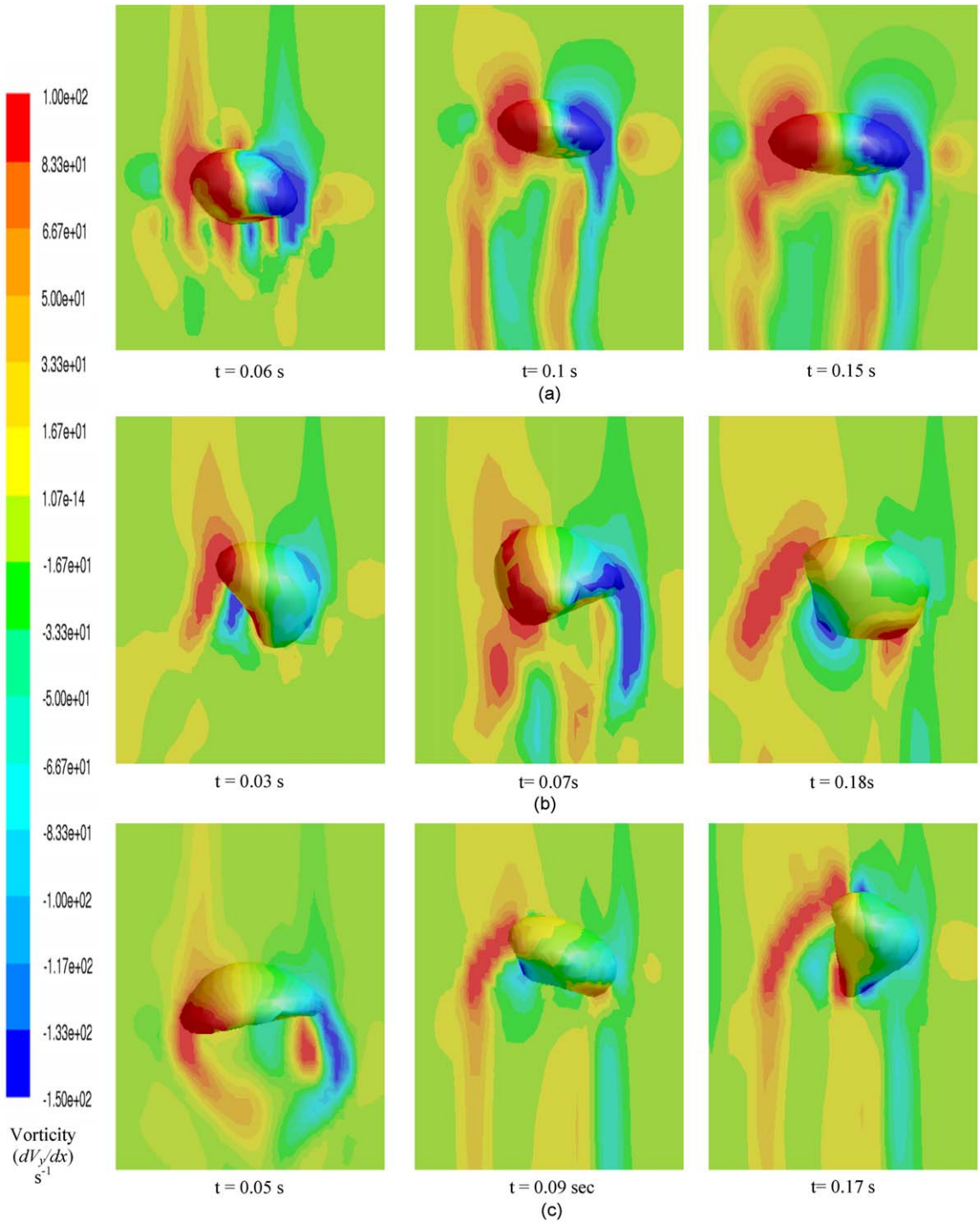

Fig. 6. Instantaneous bubble shapes and vorticity distributions for air bubbles rising in low viscosity liquid at three different instants (Liquid: water, $\omega = 6.2\,s^{-1}$) (a) $d_B = 2.84$ mm, (b) $d_B = 5.54$ mm and (c) $d_B = 8$ mm.

2.2. Solution domain, boundary conditions and numerical schemes

The spatial derivatives in Eqs. (2) and (7) were discretized using the QUICK scheme (Leonard, 1979) while a first-order implicit method was used for the discretization of the temporal derivatives. The pressure implicit with splitting of operator (PISO) algorithm (Issa, 1986) was used for the pressure–velocity coupling in the momentum equation.

Tomiyama et al. (2002) used a rectangular column with height (H) of 900 mm, width (W) of 30 mm and depth (D) of 150 mm to investigate the lift force acting on a single bubble rising in a viscous liquid imposed with a linear shear. The actual liquid height considered by Tomiyama et al. (2002) to monitor the bubble rise was 210 mm. In the present work, a 3-D rectangular solution domain ($H = 150$ mm, $W = 30$ mm, $D = 15$ mm) as shown in Fig. 1 with a uniform structured grid was used. In order to achieve a fully developed liquid flow with specified velocity gradient (shear), the required velocity profiles was imposed at the velocity inlet as shown in Fig. 1 and the outflow boundary condition was specified at the outlet. In order to reduce the computational costs, a column depth equal to

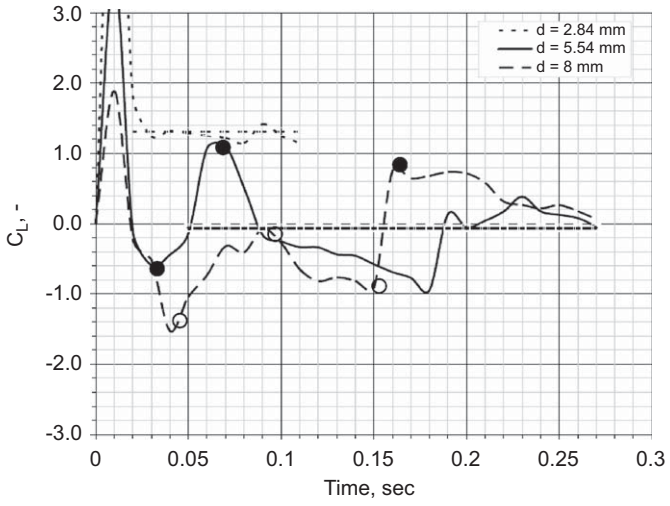

Fig. 7. Time evolution of C_L for low viscosity liquid for $d_B = 2.84$, 5.54 and 8 mm. The straight lines show the time-averaged value of C_L for each bubble and circles show the transition points. (Liquid: water, $\omega = 6.2\,s^{-1}$).

three times d_B was used by imposing the specified velocity profiles at the front and rear walls of the column as shown in Fig. 1. A no slip boundary condition was used at the both moving and stationary wall. The effect of column depth (D) on the bubble rise velocity and C_L was studied and the results are reported in Section 4.1.

To avoid the parasite currents at the interfaces, the Courant number of 0.1 was used. The effect of time step on C_L was investigated by performing the simulations with four different time steps (1×10^{-4}, 1×10^{-5}, 1×10^{-6}, and 1×10^{-7} s) and the predicted values of C_L were −0.69, −0.79, −0.82 and −0.80, respectively. The difference in predicted C_L for 1×10^{-6} and 1×10^{-7} s was about 2% and therefore all simulations were carried out using a time step of 1×10^{-6} s and Courant number of 0.1.

3. Calculation of lift coefficient

The net transversal lift force generated due to the shear and the wake effects was calculated using the simulated bubble trajectories. Following Tomiyama et al. (2002), it was assumed that both the shear induced and wake induced lift forces have the same functional form given by Eq. (1). The magnitude and direction of the total lift force can then be obtained by solving the equation of bubble motion,

$$(\rho_G + 0.5\rho_L)\frac{d\vec{V}_G}{dt} = -\frac{3}{4}\frac{C_D}{d_B}\rho_L|\vec{V}_R|\vec{V}_R - C_L\rho_L\vec{V}_R \times \nabla \times \vec{V}_L + (\rho_L - \rho_G)\vec{g} \quad (8)$$

The term on the left hand side is the inertia force, whereas the first, second and third terms on the right hand side of the Eq. (8) represent the drag, lift and buoyancy force, respectively. In the above equation, $\vec{V}_G = (V_{Gx}, V_{Gy}, 0)$ is the bubble rise velocity in a fixed reference frame which was calculated based on the displacement of the bubble center with time. $\vec{V}_L = (0, -\omega(x - W), 0)$ is the undisturbed local liquid velocity and $\vec{V}_R = \vec{V}_G - \vec{V}_L$ is the relative velocity of the bubble. ω ($=|dV_{Ly}/dx|$) is the shear rate and W is the column width. The co-ordinate system used in the present work is shown in Fig. 1. The migration of bubbles in the z-direction (along the depth) was found to be negligible. Therefore, the z-component of equation of bubble motion was not solved. The bubble rise velocity $\vec{V}_G$ can be written as,

$$\vec{V}_G = \vec{V}_R + \vec{V}_L = (V_{Rx}, V_{Ry} - \omega(x - W), 0) \quad (9)$$

The lift coefficient was calculated by solving x- and y-components of Eq. (8) with $\rho_L \gg \rho_G$.

$$0.5\rho_L\left(\frac{dV_{Rx}}{dt}\right) = -\frac{3}{4}\frac{C_D}{d_B}\rho_L|\vec{V}_R|V_{Rx} + C_L\rho_L\omega V_{Ry} \quad (10)$$

$$0.5\rho_L\left(\frac{dV_{Ry}}{dt} - \omega V_{Rx}\right) = -\frac{3}{4}\frac{C_D}{d_B}\rho_L|\vec{V}_R|V_{Ry} - C_L\rho_L\vec{V}_{Rx} + \rho_L g \quad (11)$$

when a bubble attains steady state relative velocities in x- and y-directions ($dV_{Rx}/dt = dV_{Ry}/dt = 0$), the C_L for a bubble rising with constant V_{Rx} and V_{Ry} can be calculated from Eqs. (10) and (11) with appropriate simplifications ($g/\omega \gg 0.5V_{Rx}$) (see Bothe et al., 2006),

$$C_L = \frac{g}{\omega}\left(\frac{V_{Rx}}{V_{Rx}^2 + V_{Ry}^2}\right) \quad (12)$$

when a bubble does not attain the steady state relative velocities in x- and y-directions, the time dependent C_L (t) and C_D (t) were obtained by solving Eqs. (10) and (11).

4. Results and discussion

The results are discussed in three parts. In the first part, the results of simulations performed to investigate the effects of different parameters: bubble diameter ($d_B = 2.84 - 8$ mm), liquid viscosity ($\mu_L = 1\times10^{-2} - 1\times10^{-3}$ kg m^{-1} s^{-1}) on the lift force acting on a single bubble rising in a sheared liquid ($\omega = 6.2\,s^{-1}$) are discussed. The range of d_B and μ_L considered in the present work and the corresponding dimensionless numbers (*Eo, Ga* and *Mo*) are listed in Table 1. In the later part, simulations of rise of multiple bubbles of uniform size (homogeneous bubbly flow) in a sheared liquid are presented. In the final part, results on the lift force acting on multiple bubbles of non-uniform sizes (heterogeneous bubbly flow) are discussed.

4.1. Single bubble rising in a sheared liquid

4.1.1. Effect of column depth and grid resolution

The dimensions of the experimental test section used by Tomiyama et al. (2002) for actual measurements were: $H = 210$, $W = 30$ and $D = 150$ mm. In order to reduce the computational efforts, the effect of column depth on the bubble rise velocity and C_L was investigated by performing the simulations with column depths of 3, 4, and 5 times d_B (other parameters: $H = 150$, $W = 30$, $d_B = 5.54$ mm, $\omega = 6.2\,s^{-1}$, air–water+glycerol system). Since a linear velocity profile was imposed on the front and rear walls of the column, a very small variation (3–7%) in the calculated C_L values was observed with the change in the column depth. Therefore in all the further simulations, the column depth equal to three times d_B was considered. The effect of grid resolution (cells per bubble diameter, CPD) on the predicted rise velocities, bubble shapes and consequently on the predicted values of C_L was studied by performing the simulations for $d_B = 3.52$ and 5.54 mm with CPDs of 9.23, 11 and 16 and the results are shown in Fig. 2 (air–water+glycerol system, $\mu_L = 0.019$ kg m^{-1} s^{-1}, $\omega = 6.2\,s^{-1}$). For $d_B = 3.52$ mm, the predicted C_L values were found to be 0.324, 0.282 and 0.248, respectively, against the experimental C_L of 0.28 (Tomiyama et al., 2002). For $d_B = 5.54$ mm, the grid independency of C_L was not achieved even up to 16 CPD. The computations with 32 CPD could not be performed due to limitations on computational resources.

In the literature, Bothe et al. (2006) also reported the effect of grid resolutions on the C_L for bubbles with different Eo_H using 16 CPD and 32 CPD (see Fig. 2). Similar to the predictions of Bothe et al. (2006), we also observed that the change in the C_L values with successive grid refinements was smaller for $d_B = 3.52$ mm than that observed for $d_B = 5.54$ mm. One of the main reasons for not

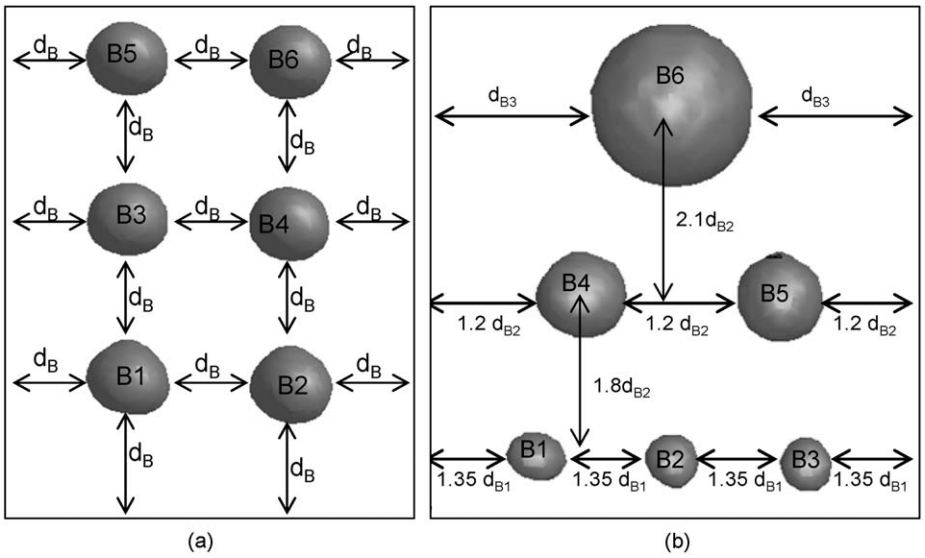

Fig. 8. Initial configurations of (a) six mono-dispersed air bubbles ($d_B = 3.52$, 5.54, 8 mm) and (b) six poly-dispersed air bubbles (3 bubbles with $d_B = 3.52$ mm [bottom row], 2 bubbles with $d_B = 5.54$ mm [middle row] and 1 bubble with $d_B = 8$ mm [top central bubble]).

achieving grid independency for larger bubbles may be the local turbulence generated in unsteady wakes behind the large bubbles. In order to achieve grid independent results for large bubbles, it may be necessary to use approaches like LES or DNS to account for the local turbulence.

4.1.2. Lift force in high viscosity systems

The effect of bubble diameter on bubble rise velocities and lift coefficients was investigated by simulating the rise of bubbles with diameters of 3.52, 5.54 and 8 mm in water+glycerol mixture. The predicted values of C_L for different d_B were plotted as a function of Eo_H (calculated based on maximum horizontal diameters d_H) as shown in Fig. 3. The predicted d_H for different bubbles with CPD of 9.23 was in a satisfactory agreement with the measured (Tomiyama et al., 2002) and predicted (Bothe et al., 2006 (obtained with CPD of 16)) values (not shown here). From Fig. 3, it can be seen that the predicted C_L of 0.32 and −0.73 for $d_B = 3.52$ and 5.54 mm, respectively (using 9.23 CPD) were over predicted as compared to predicted C_L of 0.27 and −0.6 (Bothe et al., 2006; 16 CPD) and measured C_L of 0.28 and −0.3 (Tomiyama et al., 2002), for $d_B = 3.52$ and 5.54 mm, respectively. The possible reasons for the disagreement between the measured and predicted values appear to be because of the contamination effects in the experiments, which were not included in the numerical model (see Bothe et al., 2006, for further discussion).

While the bubble size considered in the previous work was up to $d_B = 5.54$ mm, we performed the simulations for a large bubble size ($d_B = 8$ mm) which corresponds to the ellipsoidal bubble regime on the bubble shape regime diagram of Clift et al. (1978). The predicted C_L for $d_B = 8$ mm was −2.4. From Fig. 3, it can be seen that the C_L decreases linearly with Eo_H. The simulated trajectories of the bubbles with three different sizes ($d_B = 3.52$, 5.54, 8 mm) for a constant Morton number ($\log Mo = -5.3$) are shown in Fig. 4(a). It can be seen clearly from the Fig. 4(a) that the larger bubbles ($d_B = 5.54$, 8 mm) move towards the moving wall whereas the smaller bubble ($d_B = 3.52$ mm) migrates steadily towards the stationary wall. These predictions of bubble trajectories were in a good agreement with the experimental observations (Tomiyama et al., 2002).

The instantaneous bubble shapes and vorticity distributions around the bubbles are shown in Fig. 5(a, b, and c), for $d_B = 3.52$, 5.54 and 8 mm, respectively. Once the initial spherical shape was developed into ellipsoidal shape, the wake behind the bubble was symmetric about the vertical axis and a steady lateral migration of the bubble was observed. A small asymmetric vorticity distribution is visible for the bubble with $d_B = 8$ mm and as a result small oscillations can be seen in the bubble trajectory (Fig. 4(a)). Nevertheless, the lift force acting on bubbles rising in high viscosity liquid can be characterized by a single characteristics value of C_L. But in for low viscosity liquids, where the oscillations in the bubble trajectory can be significant, it may be difficult to obtain a single characteristic value of C_L. Therefore, the rise of single bubble in low viscosity liquids was investigated and results are discussed in the following section.

4.1.3. Lift force in low viscosity systems

The simulations were performed to investigate the effect of liquid viscosity ($\mu_L = 0.001\ \mathrm{kg\,m^{-1}\,s^{-1}}$) on C_L for $d_B = 2.84$, 5.54 and 8 mm. The simulated trajectories of air rising in water at a constant Morton number ($\log Mo = -10.6$) are shown in Fig. 4(b). The snapshots of instantaneous bubble shapes and vorticity distributions are shown in Fig. 6. The corresponding time dependent C_L values (calculated in fixed reference frame) are shown in Fig. 7. The trajectory of the small air bubble ($d_B = 2.84$ mm) rising in water was found to be steadily migrating towards the stationary wall even though the vorticity distribution was slightly asymmetric (see Fig. 6(a)) which may be because of small change in the bubble shape. As expected, very small fluctuations in C_L were observed for the small bubble ($d_B = 2.84$ mm) with an average C_L of 1.25 as shown in Fig. 7.

As the bubble size was increased to $d_B = 5.54$ mm, unlike for the viscous systems, the bubble was found migrate on both side (of $X^* = 0.5$) (see Fig. 4(b)). From the instantaneous bubble shapes and vorticity distributions shown at the transition points at which bubble changes its direction (see Fig. 6(b)), it can be seen the wake generated behind the bubble leads to the observed wobbling behavior. However, all the investigations of Tomiyama et al. (2002) and Bothe et al. (2006) and the earlier work fall in the ellipsoidal shape regime ($1.5 \le Eo \le 40$; $-3 \le \log Mo \le -5$) of the bubble diagram (Clift et al., 1978) where the rise behavior could be characterized by a single value of C_L. But air–water system with $\log Mo = -10.6$ and $1.5 \le Eo \le 8.72$ fall in the wobbling regime, where it was difficult to obtain a single value of C_L because of the fluctuating rise velocities in

the lateral direction. As seen in Fig. 7, the bubble initially migrated towards the high velocity region and the negative value of C_L was found to increase. But at $t = 0.03$, $t = 0.07$ and $t = 0.18$ s, the bubble deformed significantly and changed its direction of migration. As a result, C_L increased sharply to a positive value and then decreased as the bubble moved up till the next transition point. The wobbling behavior of the bubble was found to increase with increase in the size of the bubble. For $d_B = 8$ mm, the asymmetric wakes generated behind the bubbles were significantly increased (as shown in Fig. 6(c)) and a similar variation of C_L with time was observed (see Fig. 7).

From Fig. 7, it can be seen that the time-averaged value of C_L (average obtained after discarding the initial transients) for larger bubbles (d_B=5.54, 8 mm) approach to a very small value, for example, C_L=1.39, −0.06 and −0.057 for d_B=2.84, 5.54 and 8 mm, respectively. This may be because the wake behind the bubble diminishes the effect mean velocity gradient on C_L. These observations agreed well with the previous literature on lift force (Beyerlein et al., 1985).

4.2. Multiple bubbles rising in sheared liquid

4.2.1. Homogeneous (mono-dispersed) bubbles

The effect of neighboring bubbles on the lift force was investigated by simulating the rise of six mono-dispersed air bubbles ($d_B = 3.52$, 5.54, 8 mm) in water+glycerol placed in a regular array as shown in Fig. 8(a). The simulated time variation of C_L for each bubble is shown in Fig. 9. The instantaneous bubble shapes and vorticity distributions at $t = 0.1$ s are shown in Fig. 10. For the dispersion of bubbles with $d_B = 3.52$ mm, once the initial spherical shaped bubbles were deformed into the ellipsoidal bubbles (see Fig. 10(a)), the influence of the imposed shear was found to diminish due to the wake effects of individual bubbles. Once the influence of the imposed shear was decreased, the net lateral migration of bubbles was also decreased and thus instantaneous values of C_L were found to fluctuate between −0.4 and 0.6 as compared with the characteristic C_L value of 0.324 obtained for the single bubble rising under the same conditions. This clearly indicates that the interactions between the bubbles for $d_B = 3.52$ mm were negligible because of the symmetric vorticity distribution observed around the individual bubbles (Fig. 10(a)).

For $d_B = 5.54$ mm, out of the six spherical bubbles in the top row (B5 and B6) experienced the shear flow and initially migrated towards the moving wall with −ve values of C_L. The rise of bubbles in the middle and the bottom rows (B3 and B4, B1 and B2) was influenced by the wakes of the leading bubbles and therefore exhibited non −ve values of C_L in the beginning. Once the wake effects are stabilized, the bubbles were found to migrate steadily towards the moving wall (Fig. 9(b)). The instantaneous values of C_L of all the bubbles were found to fluctuate between 0.2 and −1.3 as compared with the characteristic value of C_L of −0.73 obtained for the single bubble rising under the same conditions. For $d_B = 8$ mm, a significant bubble deformation was observed (Fig. 10(c)) which led to increased interactions between the bubbles (see the ellipsoidal shape of the bubbles in the top row against the elongated shape of the bubbles in the middle and bottom rows). The instantaneous C_L was also influenced by these strong interactions between the bubbles. The time-averaged C_L of individual bubbles was found to be within −0.2 to −0.8 as compared to C_L of −2.4 obtained for a single bubble under the same conditions.

From the above simulations of mono-dispersed bubbles in a viscous liquid (gas volume fraction $\alpha_G = 3\%$ for all the three cases reported above), it was observed that with the increase in d_B, bubble shape changes from ellipsoidal to wobbling regime and the wake effects become dominant which in turn lead to the increased fluctuations in C_L. Importantly, it should be noted that with increase in the number of bubbles, the number-average of time-averaged C_L of all bubbles was found to decrease significantly. The number-averaged

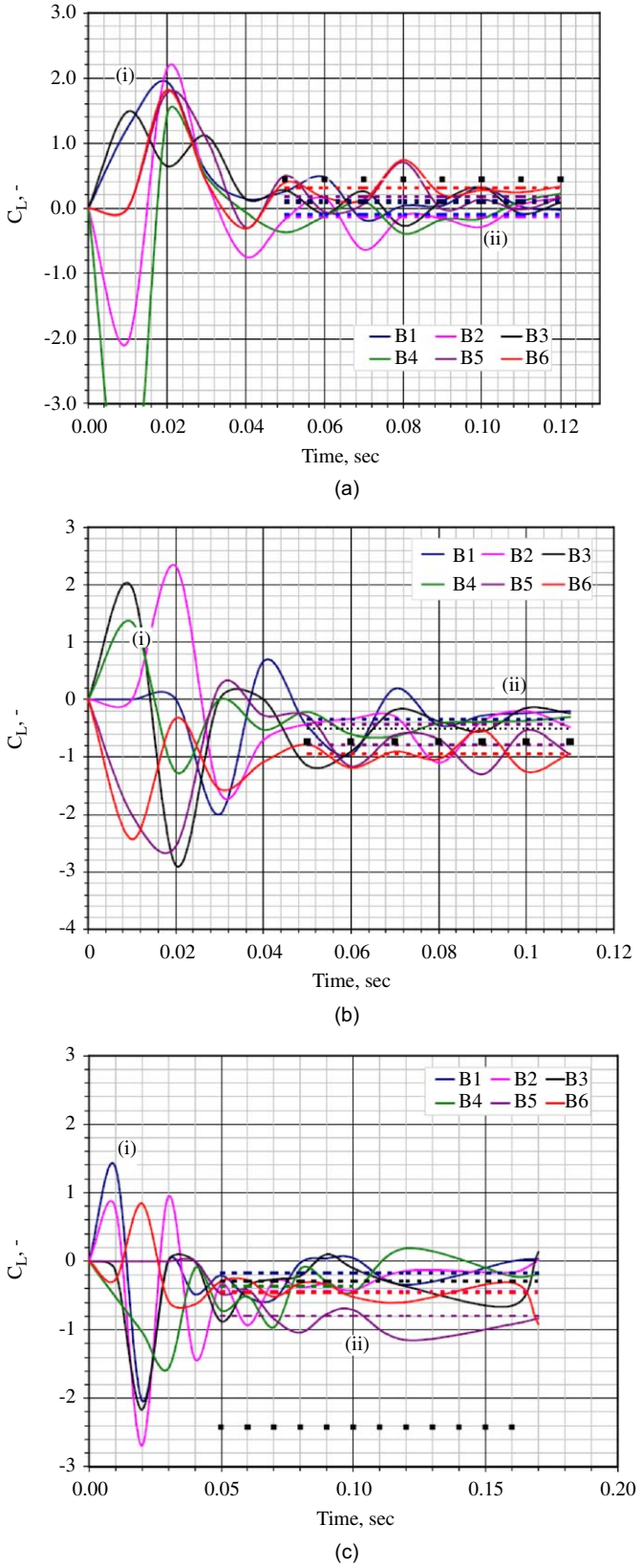

Fig. 9. Time evolution of C_L for six mono-dispersed air bubbles rising in water+glycerol for (a) $d_B = 3.52$ mm, (b) $d_B = 5.54$ mm and (c) $d_B = 8$ mm ($\omega = 6.2\,s^{-1}$). The dotted lines show the time-averaged value of C_L for individual bubbles and square points show the predicted C_L for a single bubble in the same system.

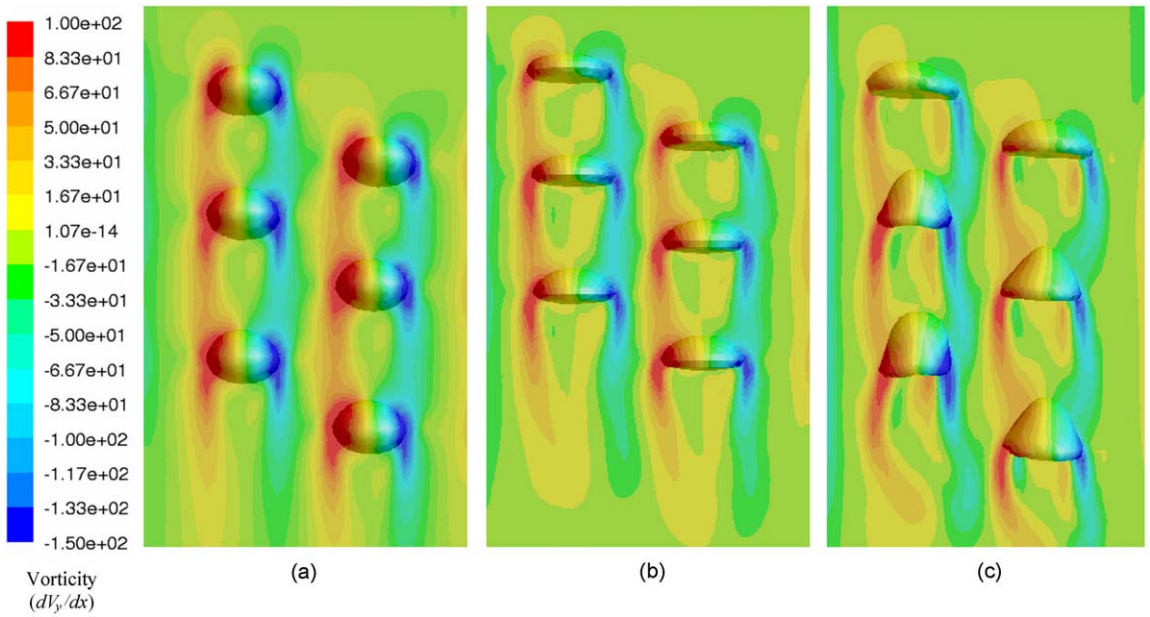

Fig. 10. Instantaneous bubble shapes and vorticity distributions for six mono-dispersed bubbles rising in water+glycerol at $t = 0.1$ s (a) $d_B = 3.52$ mm, (b) $d_B = 5.54$ mm and (c) $d_B = 8$ mm ($\omega = 6.2\,s^{-1}$).

and time-averaged C_L values were 0.071, −0.581, −0.417 for the dispersions with $d_B = 3.52$, 5.54 and 8 mm, respectively, and the corresponding C_L valued for the single bubble rise were 0.32, −0.73 and −2.4 for $d_B = 3.52$, 5.54 and 8 mm, respectively. Thus our simulations confirm that hypothesis of Beyerlein et al. (1985) and Behzadi et al. (2004) that the C_L decreases sharply with a moderate increase in the volume fraction.

4.2.2. Heterogeneous (poly-dispersed) bubbles

In order to investigate the lift force in poly-dispersed systems, the simulation of rise of six bubbles of different diameters (d_{B1}=3.52 mm, $d_{B2} = 5.54$ mm, $d_{B3} = 8$ mm) in sheared water+glycerol in an irregular array with the arrangement shown in Fig. 8(b) was performed. The time variation of C_L values for individual bubbles along with their time average is shown in Fig. 11(a). The instantaneous bubble shapes and vorticity distributions at three different instants are shown in Fig. 11(b). The rise behavior of each bubble in the heterogeneous dispersion was completely different from that of a single bubble rise. The wake induced by the large central bubble (B6, $d_B = 8$ mm) was found to influence the lateral migration of bubbles in the middle row. The rise of bubble B4 ($d_B = 5.54$ mm) was strongly influenced by the large central bubble B6 as it enters the wake of the central bubble (snapshot (i)) and its time-averaged C_L was found to be 1.04 against the C_L of −0.73 obtained for single bubble rising under same shear rate. The C_L of the bubble B4 reaches its minimum value of 0.41 just before it coalesces with the large bubble B6 at $t = 0.16$ s (as shown in snapshot (ii)). The instantaneous C_L of B6 was found to fluctuate between −3 and −1 with the time-averaged value of −2.3 which was comparable with the C_L of −2.5 obtained for the single bubble rising under same shear rate. Since the rise of leading large bubble B6 was not much influenced by the presence of other bubbles, the shear-induced lift on the large bubble dominated over wake induced lift and the bubble B6 migrated towards the moving wall. As a result, the distance of B6 from the bubble B5 ($d_B = 5.54$ mm), which was near the stationary wall, increased and thus rise of B5 was less affected by the leading central bubble as that compared to B4 near the moving wall. But later, as the large bubble B6 moved upwards, it was deformed into a spherical cap shape and the following bubbles (B5 and B1) were pulled by the strong wake induced by the central bubble (clearly seen in the snapshot (iii)). From Fig. 11(a), it can be seen that initially C_L of the bubble B5 was oscillating between −4 and −2, but as it was trying to catch up the leading bubble C_L was increased to −0.38 (snapshot (iii)) just before it coalesced with the central bubble.

Similarly, smaller bubbles ($d_{B1} = 3.52$ mm) in the bottom row (B1, B2 and B3) were also found to experience the wake effects of the leading bubbles (more of B6 than that of B4 and B5), which is clearly visible in their C_L behavior. The average C_L of bubble bubble (B1, B2 and B3) was found to be 1.2, −0.13 and −0.6 as compared to C_L of 0.324 for single bubble rise under same shear rate. Since B1 was near to the moving wall, it experienced more effect of the leading bubbles as compared to B2 and B3. This is evident from the instantaneous C_L values for B1 which were found to fluctuate between 0.5 and 2.5. As the large bubble B6 moved very fast towards the high velocity region, the distance between B3 and B6 increased, therefore B3 experienced the least effect of the wake induced by B6 (as seen in snapshot (iii)). The number- and time-averaged C_L of all the poly-dispersed was found to −0.58, which was comparable with the number- and time-averaged value of (0.07, −0.58, −0.41 for $d_B = 3.52$, 5.54 and 8 mm) mono-dispersed system especially with large bubbles.

5. Conclusions

The lift force acting on both single/multiple bubbles in linear shear flow of liquid with different properties was numerically investigated using the VOF method. The rise of single bubbles in sheared viscous liquid (corresponding to the ellipsoidal regime, $2.35 \leq Eo \leq 11.68$ and $\log Mo = -5.3$) was simulated and the predicted C_L values were compared with the measurement of Tomiyama et al. (2002). Further, the lift force acting on single bubbles rising in low viscosity liquid (corresponding to the wobbling regime, $1.1 \leq Eo \leq 8.72$, $-10.6 \leq \log Mo \leq -14.6$) was investigated. The effect of neighboring bubbles on the lift force was investigated by simulating the rise of six homogeneous (mono-dispersed) and

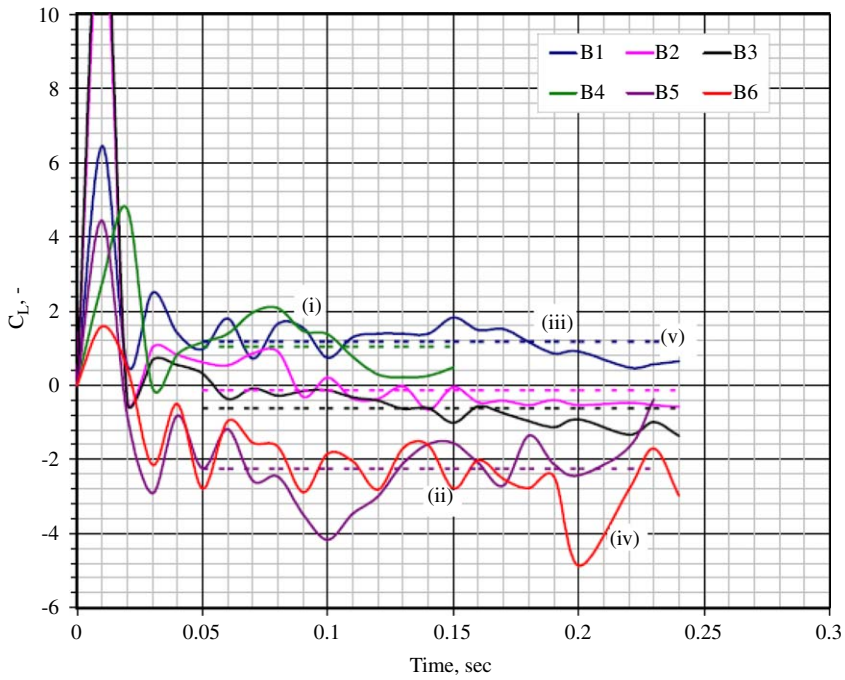

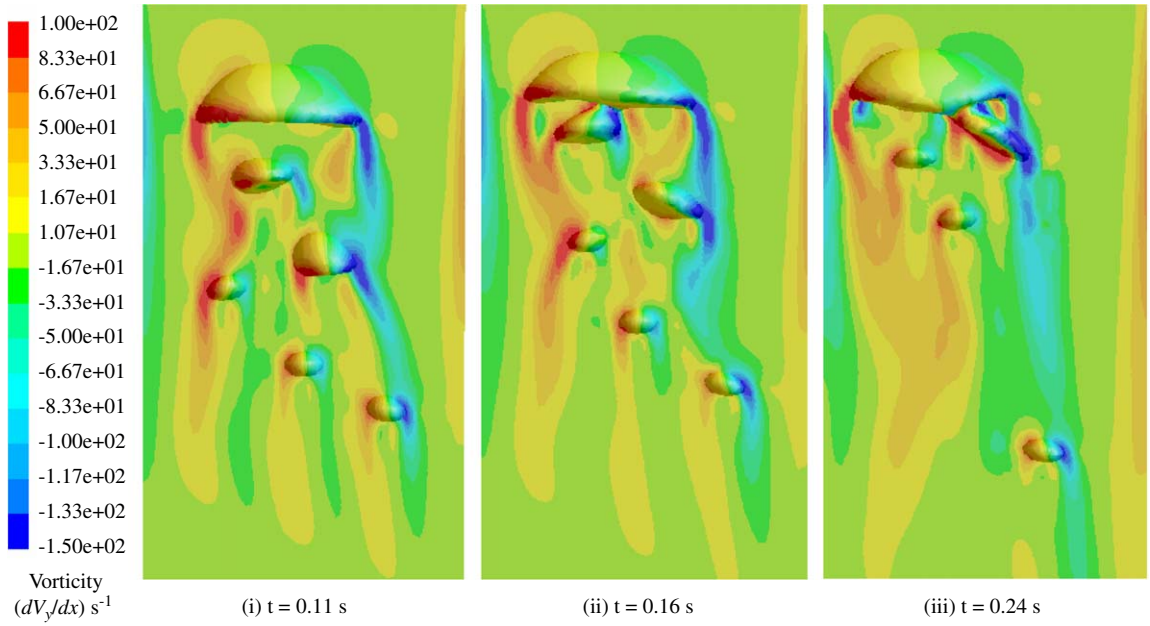

Fig. 11. (a) Time evolution of C_L for six poly-dispersed air bubbles of three different sizes 3.52, 5.54, 8 mm rising in water+glycerol ($\omega = 6.2\,s^{-1}$). The dotted lines show the time-averaged value of C_L for individual bubbles and (b) instantaneous bubble shapes and vorticity distributions.

heterogeneous (poly-dispersed) bubbles in a viscous liquid. The key conclusions of the present work are as follows.

- For highly viscous system like air–water+glycerol (corresponding to the ellipsoidal regime), a single characteristic value of C_L was observed and C_L was found to vary linearly with Eo_H which agreed well with the correlations of Tomiyama et al. (2002) and Bothe et al. (2006).
- For low viscosity systems like air–water (corresponding to the wobbling regime), the bubble was found to oscillate in the lateral direction exhibiting fluctuating values of C_L. These fluctuations in C_L were found to increase with increase in d_B. The time-averaged value of C_L for the bubbles in the wobbling regime was found to approach to a very small value with increase in d_B.
- For both mono-dispersed and poly-dispersed bubbles rising in viscous liquids, bubble–bubble interactions and therefore fluctuations in C_L were found to increase with increase in d_B for the same volume fraction. The number- and time-averaged C_L of all the bubbles was found to be very small as compared to the characteristic C_L value of the single bubble for the corresponding d_B.

Thus, our simulations confirm the hypothesis of Beyerlein et al. (1985) and Behzadi et al. (2004) that value of C_L decreases sharply with a moderate increase in the volume fraction.

It should be noted that the multiple bubbles simulations reported here correspond to the volume fraction of 3%. Systematic investigations of the effect of volume fraction on the mean C_L with appropriate experimental validation will be useful to develop the closures for lift force for homogeneous and heterogeneous bubble dispersions.

Notation

C_D, C_{Do}	drag coefficient, drag coefficient of a single bubble, respectively, dimensionless
C_L	lift coefficient, dimensionless
d_B, d_H	sphere equivalent and horizontal bubble diameter, respectively, mm
D	column depth, mm
Eo, Eo_H	Eotvos number ($=g\Delta\rho d_B^2/\sigma$) and horizontal Eotvos number ($=g\Delta\rho d_H^2/\sigma$), respectively, dimensionless
$\vec{F}$	surface tension force, kg m^{-2} s^{-2}
$\vec{F}_D$, $\vec{F}_L$, $\vec{F}_{VM}$	drag, lift and virtual mass force, respectively, kg m^{-2} s^{-2}
$\vec{F}_{GL}$	total interfacial force, kg m^{-2} s^{-2}
Fr	Froude number, dimensionless
g	gravitational constant, m s^{-2}
Ga	Galileo number ($=\rho_L^2 g d_B^3/\mu^2$), dimensionless
H	column height, mm
Mo	Morton number ($=g\Delta\rho\mu_L^4/\rho_L^2\sigma^3$), dimensionless
n_B	number of bubbles, dimensionless
$n, \hat{n}$	surface normal and unit normal vector, respectively, dimensionless
P	pressure, Pa
Re	Reynold number ($=\rho_L\|V_R\|d_B/\mu_L$), dimensionless
t	time, s
$\vec{V}$, $\vec{V}_R$	velocity and relative velocity, respectively, m s^{-1}
W	column width, mm
X, X^*	dimensional and dimensionless (X/W) horizontal coordinate, respectively
Y, Y^*	dimensional and dimensionless (Y/W) vertical coordinate, respectively

Greek letters

α	volume fraction, dimensionless
κ	surface curvature, dimensionless
μ	molecular viscosity, Pa s
ρ	density, kg m^{-3}
σ	surface tension, Nm^{-1}
ω	shear rate, s^{-1}

Subscripts and superscripts

G, L	gas and liquid, respectively
P, q	primary and secondary phase, respectively
X, y	horizontal and vertical direction, respectively

Acknowledgments

One of the authors (SSR) is grateful to Ministry of Human Resource Development, India for providing the research fellowship.

References

Auton, T.R., 1987. The lift force on a spherical body in a rotational flow. Journal of Fluid Mechanics 183, 199–218.
Behzadi, A., Issa, R.I., Rusche, H., 2004. Modelling of dispersed bubble and droplet flow at high phase fractions. Chemical Engineering Science 59, 759–770.
Beyerlein, S.W., Cossmann, R.K., Richter, H., 1985. Prediction of bubble concentration profiles in vertical turbulent two-phase flow. International Journal of Multiphase Flow 11, 629–641.
Bothe, D., Schmidtke, M., Warnecke, H.J., 2006. VOF-simulation of the rise behavior of single air bubbles in linear shear flows. Chemical Engineering and Technology 29, 1048–1053.
Brackbill, J.U., Kothe, D.B., Zemach, C., 1992. A continuum method for modeling surface tension. Journal of Computational Physics 100, 335.
Bunner, B., Tryggvason, G., 2002. Dynamics of homogeneous bubbly flows: part 1: rise velocity and microstructure of the bubbles. Journal of Fluid Mechanics 466, 17–52.
Buwa, V.V., Ranade, V.V., 2002. Dynamics of gas–liquid flow in rectangular bubble columns: experiments and single/multi-group simulations. Chemical Engineering Science 57, 4715–4736.
Clift, R., Grace, J.R., Weber, M.E., 1978. Bubbles, Drops and Particle. Academic Press, New work.
Hibiki, T., Ishii, M., 2007. Lift force in bubbly flow systems. Chemical Engineering Science 62, 6457–6474.
Hirt, C.W., Nichols, B.D., 1981. Volume of fluid (VOF) method for the dynamics of free boundaries. Journal of Computational Physics 39, 201–225.
Ishii, M., Zuber, N., 1979. Drag coefficient and relative velocity in bubbly droplet or particulate flows. AIChE Journal 25, 843–855.
Issa, R.I., 1986. Solution of the implicitly discretised fluid flow equations by operator splitting. Journal of Computational Physics 62, 40–65.
Kariyasaki, A., 1987. Behavior of a single gas bubble in a liquid flow with a linear velocity profile. In: Proceedings of the 1987 ASME/JSME Thermal Engineering Conference, pp. 261–267.
Krishna, R., Urseanu, M.I., Van Baten, J.M., Ellenberger, J., 1999. Rise velocity of a swarm of large gas bubbles in liquids. Chemical Engineering Science 54, 171–183.
Legendre, D., Magnaudet, J., 1998. The lift force on a spherical bubble in a viscous linear shear flow. Journal of Fluid Mechanics 368, 81–126.
Leonard, B.P., 1979. A stable and accurate convective modelling procedure based on quadratic upstream interpolation. Computer Methods in Applied Mechanics and Engineering 19, 59–98.
Magnus, G., 1853. Ueber die Abweichung der Geschosse, und: Ueber eine auffallende Erscheinung bei rotirenden Korpern. Annalen der physik 164, 1–29.
Rafique, M., Chen, P., Dudukovic, M.R., 2003. Computational modelling of gas liquid flow in bubble column. Reviews in chemical engineering 20, 225.
Rampure, M.R., Buwa, V.V., Ranade, V.V., 2003. Modelling of gas–liquid/gas–liquid–solid flows in bubble columns: experiments and CFD simulations. Canadian Journal of Chemical Engineering 81, 692–706.
Rider, W.J., Kothe, D.B., 1998. Reconstructing volume tracking. Journal of Computational Physics 141, 112–152.
Saffman, P.G., 1965. The lift on a small sphere in a slow shear flow. Journal of Fluid Mechanics 22, 385.
Sankaranarayanan, K., Shan, X., Kevrekidis, I.G., Sundaresan, S., 2002. Analysis of drag and virtual mass forces in bubbly suspensions using an implicit formulation of the lattice Boltzmann method. Journal of Fluid Mechanics 452, 61–96.
Sankaranarayanan, K., Sundaresan, S., 2002. Lift force in bubble suspensions. Chemical Engineering Science 57, 3521–3542.
Sridhar, G., Katz, J., 1995. Drag and lift forces on microscopic bubbles entrained by a vortex. Physics of Fluids 7, 389–399.
Tomiyama, A., Tamai, H., Zun, I., Hosokawa, S., 2002. Transverse migration of single bubbles in simple shear flows. Chemical Engineering Science 57, 1849–1858.
Žun, I., 1980. The transverse migration of bubbles influenced by walls in vertical bubbly flow. International Journal of Multiphase Flow 6, 583–588.